Microporous and Mesoporous Materials 133 (2010) 1–9

Contents lists available at ScienceDirect

Microporous and Mesoporous Materials

journal homepage: www.elsevier.com/locate/micromeso

Factorial design to optimize microwave-assisted synthesis of FDU-1 silica with a new triblock copolymer

L.C. Cides da Silva [a,*,1], T.V.S. dos Reis [a], I.C. Cosentino [b], M.C.A. Fantini [c], J.R. Matos [a], R.E. Bruns [d]

[a] Departamento de Química Fundamental, Instituto de Química, Universidade de São Paulo, C.P. 66083, 05508-000 São Paulo, SP, Brazil
[b] Instituto de Pesquisas Energéticas e Nucleares-IPEN, Av. Prof. Lineu Prestes, 2242, 05508-000 São Paulo, SP, Brazil
[c] Departamento de Física Aplicada, Instituto de Física, Universidade de São Paulo, CP 66318, 05314-970 São Paulo, SP, Brazil
[d] Instituto de Química, Universidade Estadual de Campinas, CP 6154, 13083-970 Campinas, SP, Brazil

ARTICLE INFO

Article history:
Received 20 August 2009
Received in revised form 6 January 2010
Accepted 8 January 2010
Available online 24 February 2010

Keywords:
FDU-1 silica
Factorial design
Microwave-assisted synthesis
Mesoporous

ABSTRACT

The synthesis of FDU-1 silica with large cage-like mesopores prepared with a new triblock copolymer Vorasurf 504® $(EO)_{38}(BO)_{46}(EO)_{38}$ was developed. The hydrothermal treatment temperature, the dissolution of the copolymer in ethanol, the HCl concentration, the solution stirring time and the hydrothermal treatment time in a microwave oven were evaluated with factorial design procedures. The dissolution in ethanol is important to produce a material with better porous morphology. Increases in the hydrothermal temperature (100 °C) and HCl concentration (2 M) improved structural, textural and chemical properties of the cubic ordered mesoporous silica. Also, longer times induced better physical and chemical property characteristics.

1. Introduction

Since the 70s different strategies have been developed to synthesize zeolites using a template-driven agent [1]. By the beginning of the 90s investigations by Mobil Oil Corporation discovered a new family of molecular sieves called M41S [2,3] opening up a new research area. These mesoporous (aluminate) silicate materials, with pore sizes in the 2–10 nm range exceeded the barrier by microporous zeolites. The preparation of mesoporous silicates requires at least three reagents in appropriate amounts: a silica source (like TEOS), a surfactant (template) and a solvent (usually water). Other reagents, such as: acids, bases, salts, swellings agents and co-solvents can also be used. Depending on the reagent amounts, the material structure can be a hexagonal phase (MCM-41), a cubic phase (MCM-48) or a lamellar phase (MCM-50), which is unstable to thermal treatment. In 1998, a new class of ordered porous materials was developed using new templates based on block copolymers [4,5]. These structures were identified as cubic (SBA-11), hexagonal 3D (SBA-12), hexagonal 2D (SBA-15) and cage-like cubic (SBA-16) structures, with pore sizes in the 5–30 nm range. These high ordered mesostructures present thicker walls and are hydrothermal and thermal stable. Yu and co-workers [6,7], using an acid medium and a triblock copolymer template with a more hydrophobic character, PEO–PBO–PEO, produced a highly ordered cage-like cubic structure, with outstanding hydrothermal stability [8] and with 12 nm pores, called FDU-1. The analysis of the mechanisms involved in the synthesis of these materials requires the optimization of several experimental factors including temperature, pH, precursors, additives, surfactants and concentrations of the reagents, which certainly affect the chemistry of the interface in the reaction mixture and, therefore, the physical–chemical nature of the products [9–11]. Many synthesis routes, that also affect the final product, were developed. One the most recent advances is the synthesis of ordered mesoporous materials with microwave-assisted hydrothermal treatment [12–15]. Among the advantages of this type of heat treatment are the high heating rate, the increase on reaction velocity, the formation of new phases and the prevalence of a selective phase over another, due to the intrinsic characteristics of dielectric heating.

The application of statistical tools such as the factorial design is also used to optimize synthetic processes, improving the structural and textural properties of, for example, microporous zeolites and silica xerogel, used as matrices in optical chemical sensors [16–18].

The synthesis of MCM-41 silica has been studied using a 2^{8-4} fractional factorial design to verify the influence of different experimental variables on product properties. Several interactions were

* Corresponding author. Tel.: +55 11 3091 3837x232; fax: +55 11 3091 3837.
E-mail addresses: lccides@iq.usp.br, luiscides@uol.com.br (L.C. Cides da Silva).
[1] Departamento de Química Fundamental, Instituto de Química da Universidade de São Paulo, P.O. Box 26077, São Paulo 05513–970, Brazil. Tel.:+55 11 3091 2166; fax:+55 11 3091 2187.

1387-1811/$ - see front matter © 2010 Elsevier Inc. All rights reserved.
doi:10.1016/j.micromeso.2010.01.005

found to be significant with pH being the most important variable [19].

More recently the effect of the synthesis conditions on the structural and textural properties of SBA-15 silica was studied using a full 2^3 factorial design. The statistical analysis showed that both synthesis conditions and aging temperature had significant influences on the properties of SBA-15 [20].

In this work, the influence of the experimental variables on the sorption and structural properties of cubic cage-like mesoporous FDU-1 silica was analyzed by the response surface method (RSM), based on factorial designs [21–26]. Statistical factorial and central composite designs for the microwave-assisted synthesis were executed using a new template, the triblock copolymer – Vorasurf 504®, with an average $(EO)_{38}(BO)_{46}(EO)_{38}$ composition. The effects of changing the HCl concentration, the presence or absence of ethanol to dissolve the polymer, and the hydrothermal microwave oven temperature were investigated, with fixed microwave 60 min heating and 24 h stirring times [12]. The microwave heating time and the stirring time were also analyzed in a subsequent factorial design. Thermogravimetry and its derivative (TG/DTG), small angle X-ray scattering (SAXS) and nitrogen sorption isotherm data were used to characterize the samples.

2. Materials and methods

2.1. Synthesis

(a) The first synthesis of FDU-1 silica was prepared based on a 2^3 factorial design. The synthesis was carried out using the same gel composition as reported by Yu et al. [6,7]: 1TEOS:0.00755;Vorasurf 504®:6HCl:155H_2O, where TEOS stands for tetraethyl orthosilicate from Aldrich Chemical Company and Vorasurf 504® is a poly(ethylene oxide)–poly(butylene oxide)–poly(ethylene oxide) triblock copolymer PEO–PBO–PEO from Dow Chemicals, with an average $(EO)_{38}(BO)_{46}(EO)_{38}$ composition. Vorasurf 504® substitutes the former B50–6600, with an average $(EO)_{39}(BO)_{47}(EO)_{39}$ composition. This new triblock copolymer has its hydroxyl content equal to 0.515 and for the B50–6600 it is 0.485. These slight differences in molar weight and hydroxyl content make Vorasurf 504® less soluble in the acid solution than B50–6600. Vorasurf 504® is an opaque viscous liquid (3570 cps. @ 25 °C) while B50–6600 is a pasty solid at room temperature.

In a standard synthesis procedure, 2 g of Vorasurf 504® copolymer and 120 g of HCl, at a pre-determined concentration, were used. The solution was stirred at room temperature until a homogeneous mixture was obtained. Subsequently, 8.32 g of TEOS was added and the resulting mixture was stirred vigorously in an open beaker for a given period of time. Precipitation was observed 30–40 min after the addition of TEOS.

In this experiment, the synthesis was carried out with and without alcohol dissolution of the polymer, varying the HCl concentration (0.2 and 2 M), with a constant 24 h stirring time and adjusting the microwave oven (mw) temperature (60 and 100 °C) for the hydrothermal treatment, at a constant time of 60 min, as shown in Table 1. Microwave irradiation was performed using a microwave oven cavity from Anton Parr model Multiwave 3000. The precipitate was filtered out, washed with distilled water, dried at 25 °C and calcinated under nitrogen, which was later switched to air, at 540 °C [12].

(b) The second synthesis was prepared based on a 2^2 factorial design with a central reference point, using the stirring and microwave times as variable parameters. The synthesis was carried out using the same procedure as described above, with the dissolution of the copolymer in ethanol and 2 M HCl solution. After TEOS was added, the resulting mixture was stirred ("st") vigorously in an open beaker for periods of 4.6 h < t_{st} < 27.3 h at 25 °C. The mixture was transferred to a Teflon® vessel, and heated under autogenous pressure. For each synthesis route at 100 °C, the time inside the microwave oven was varied (48 min < t_{mw} < 132 min), as shown in Table 2. Microwave irradiation was performed using a Microsynth Labstation for microwave-assisted synthesis (Milestone Inc). Identical to the first synthesis, the precipitate was filtered out, washed with distilled water and dried at 25 °C and calcinated under nitrogen, which was later switched to air, at 540 °C.

Both sample preparation and their characterization measurements were performed in random order.

Table 1
The experimental parameters and their high and low levels of the 2^3 factorial design for the microwave – assisted synthesis of FDU-1 silica. The X_i's are the codified factor levels.

Experiments	HCl (mol L^{-1})	Ethanol (mL)	Temperature (°C)	X_1	X_2	X_3
1	0.2	Absence	60	–	–	–
2	2.0	Absence	60	+	–	–
3	0.2	Presence	60	–	+	–
4	2.0	Presence	60	+	+	–
5	0.2	Absence	100	–	–	+
6	2.0	Absence	100	+	–	+
7	0.2	Presence	100	–	+	+
8	2.0	Presence	100	+	+	+

2.2. Themogravimetry/thermogravimetry derivative (TG/DTG)

TG/DTG/T curves were obtained on a Model TGA51 thermogravimetric analyzer (Shimadzu) using a sample mass of ~15 mg in a Pt crucible, with a heating rate of 5 °C min^{-1} up to 540 °C in a dynamic N_2 atmosphere (50 mL min^{-1}). Then the atmosphere was switched to air. The samples were kept at 540 °C for 30 min and subsequently heated to 1200 °C at a heating rate of 10 °C min^{-1}.

2.3. Small angle X-ray scattering (SAXS)

The SAXS curves were obtained at the Brazilian Synchrotron Light Laboratory (LNLS), Campinas, SP, Brazil, using the D11A-SAXS beamline [27,28]. The white photon beam was extracted from the ring through a high-vacuum path. After passing through a thin beryllium window, the beam was monochromatized and horizontally focused by a cylindrically bent and asymmetrically cut (1 1 1) silicon single crystal. The selected wavelength was 0.1608 nm. The focus was located at the detection plane. The scattered intensities were collected by an one-dimensional position sensitive detector, at a distance from the sample holder such that the scattering vector was selected as 0.02 nm^{-1} < q < 3.5 nm^{-1}. An ionization

Table 2
The experimental conditions of the central composite design. X_1 and X_2 represent the codified levels of stirring and microwave times.

Experiments	Stirring time (h)	Microwave time (min)	X_1	X_2
1	6	60	–	–
2	24	60	+	–
3	6	120	–	+
4	24	120	+	+
5	15	90	0	0
6	15	90	0	0
7	15	90	0	0
8	4.6	90	$-\sqrt{2}$	0
9	18	132	0	$\sqrt{2}$
10	27.3	90	$\sqrt{2}$	0
11	18	48	0	$-\sqrt{2}$

detector monitored the intensity of the incident beam. The data were corrected for detector homogeneity, incident beam intensity, sample absorption and blank subtraction (sample holder with two mica windows). A straight line background was removed from each diffraction peak of all SAXS data.

2.4. Nitrogen sorption isotherms

Nitrogen sorption isotherms were measured with Micromeritics ASAP 2010 volumetric sorption analyzer using 99.998 % pure nitrogen. Measurements were performed in the relative pressure range from 10^{-6} to 0.99 liquid nitrogen on samples degassed for 2 h, under reduced pressure at 200 °C. The specific surface area was evaluated using the BET method [29]. The total pore volume was estimated from the amount adsorbed at the relative pressure of 0.99. The pore size distribution (PSD) was calculated using the BJH algorithm [30], with the relation between the capillary condensation pressure and the pore diameter established by Kruk, Jaroniec and Sayari (KJS) [31].

2.5. Structural and textural parameters obtained from nitrogen sorption and SAXS

The pore diameter (W_d) was calculated using a geometrical equation proposed by Ravikovitch and Neimark [32] for materials with cubic structure with *Fm3m* symmetry [33,34].

$$W_d = a\left(\frac{6\ \varepsilon_{me}}{\pi v}\right)^{1/3} \quad (1)$$

Here a is the unit-cell parameter determined from the SAXS results, v is the number of spherical pores per unit cell ($v = 4$ for the fcc structure) and ε_{me} is the volume fraction of ordered mesoporous in the structure given by

$$\varepsilon_{me} = \left(\frac{\rho V_p}{1+\rho(V_p+V_m)}\right) \quad (2)$$

where ρ is the pore wall density, assumed to be equal to 2.2 g cm^{-3}, which is typical of amorphous silica frameworks. V_p is the total primary mesopore volume and V_m is the micropore volume, both obtained from the N_2 sorption data. The average pore wall thickness b in the fcc structure is determined as:

$$b = \frac{W_d(1-\varepsilon_{me})}{3\ \varepsilon_{me}} \quad (3)$$

2.6. Statistical methods

Statistical factorial and central composite designs allow systematic studies of how responses properties that characterize systems are affected by manipulated factors [21,22]. The designs are efficient since they require execution of only a small number of experiments. They are orthogonal designs and hence provide reliable results for the quantitative effects of factor changes on response values of interest. The effect values are determined by linear regression least squares procedures and can be calculated from the matrix equation

$$\mathbf{B} = \mathbf{X}'\mathbf{X}^{-1}\mathbf{X}\mathbf{Y} \quad (4)$$

where $\mathbf{X}$ is the design matrix containing the factor levels and $\mathbf{Y}$ is the corresponding matrix containing the response values. The $\mathbf{B}$ matrix contains the model coefficients with the linear, quadratic and interaction effect values of the factors on the responses. Errors in these effect values can be calculated from the equation

$$Vb = \mathbf{X}'\mathbf{X}^{-1}s_r^2 \quad (5)$$

where $V(b)$ represents the variances of the model coefficients for the response value of column b of the $\mathbf{B}$ matrix.

Principal components [23,24] are obtained by diagonalizing the covariance or the correlation matrix, $\mathbf{Z}'\mathbf{Z}$ [24]. $\mathbf{Z}$ is an experimental data matrix consisting of n rows, one for each experiment of the experimental design, and p columns, one for each manipulated factor and response that characterizes the system being studied. The elements of the $\mathbf{Z}$ matrix are the values of the factor levels of the experiments and the response values measured for the experiments, $\mathbf{Z} = (\mathbf{X}\vdots\mathbf{Y})$. On diagonalizing $\mathbf{Z}'\mathbf{Z}$ a small number of principal components are selected that are capable of describing a large portion of the data variance. Ideally the variance of the selected components describes signal whereas that of the discarded components pertain to noise. For the principal component model

$$\mathbf{Z} = TP^t + \varepsilon \quad (6)$$

where the product of scores and loadings, T and P^t, are expected to contain useful information and ε, the noise. The loading matrix contains elements that are correlation coefficients between the principal components and the original variables. It shows how the manipulated factor levels are correlated with the response values. The score matrix contains information about the experiments that have been performed and can be useful for optimizing systems with large numbers of responses.

3. Results and discussion

Previous synthesis of FDU-1 silica using B50–6600 [12,33] provided large microporous volume, surface area and pore diameter, compared to the values attained with Vorasurf 504®. The smaller molar mass of the new triblock copolymer compared to B50–6600 explains these results. The decrease of microporous volume is a positive result concerning the catalytic applications of this material.

In order to present an example of the data obtained for the analyzed samples of the full 2^3 factorial design, a TG/DTG/T curve, a SAXS pattern, and a N_2 sorption isotherm are presented in Figs. 1–3, respectively. The thermogravimetric analysis provided a profile similar to a previous study with the B50–6600 copolymer [15], where physically adsorbed water release, copolymer decomposition, carbonaceous compound release and silanol decomposition were observed as the temperature increased. All the SAXS data that presented diffraction peaks are assigned to a cubic *Fm3m* structure, typical of FDU-1; also, the N_2 sorption isotherms present the typical shape of the cage-like structure [12].

A 2^3 factorial design was carried out to investigate the effects of changing the HCl concentration from 0.2 to 2.0 mol L^{-1}, the

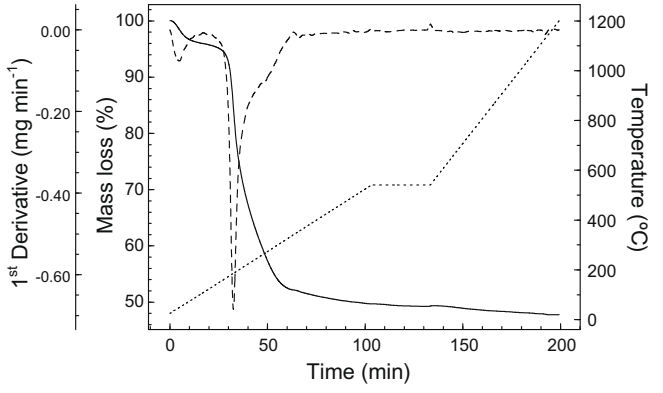

Fig. 1. TG/DTG/T results obtained for sample number 6 of the full 2^3 factorial design.

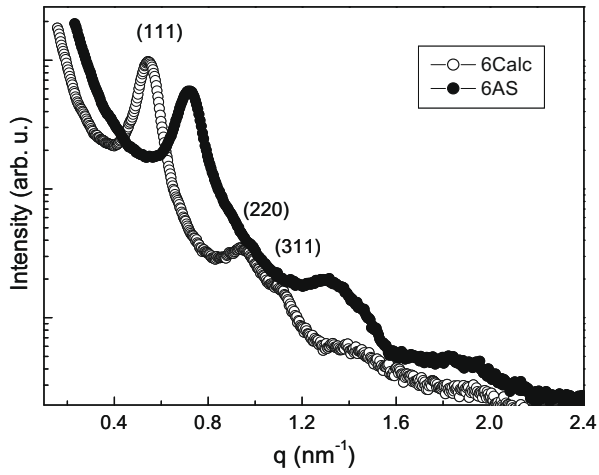

Fig. 2. Small angle X-ray scattering (SAXS) patterns for as-synthesized and calcined sample number 6 of the full 2^3 factorial design.

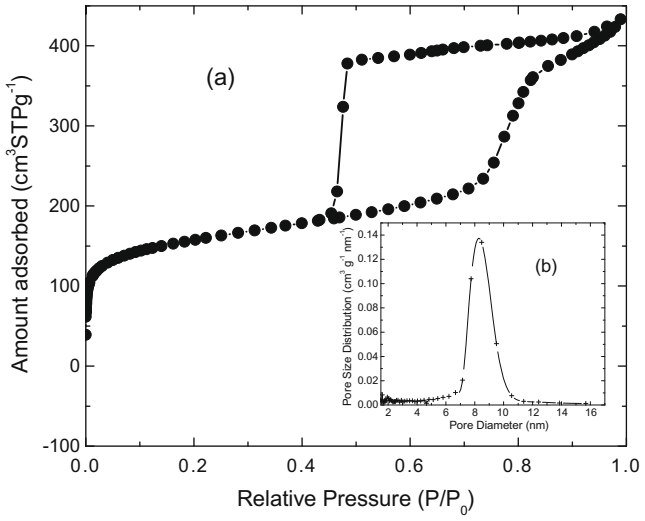

Fig. 3. (a) Nitrogen sorption isotherm at -196 °C and (b) the corresponding pore size distributions for sample number 6 of the full 2^3 factorial design.

presence or absence of ethanol, and 60 and 100 °C microwave hydrothermal treatment temperatures on the chemical, textural and structural properties of silica with large cage-like mesoporous 3 D, FDU-1 type samples. As indicated in Table 1 all possible combinations of the two levels for the three factors are included in the design. Duplicate results for the textural and structural properties are presented in Table 3. Note that the experiments carried out at 0.2 mol L^{-1} and 100 °C in the presence of ethanol did not furnish results for AS (*a*, lattice parameter of as-synthesized sample), Calc (*a*, lattice parameter of calcined sample) and *b* (wall thickness), because the samples did not present ordered mesoporous structures.

Corresponding results for the thermogravimetric analyses are presented in Table 4. The temperature change provoked 95% confidence level significant effects on S_{BET} (146 ± 38), V_{PT} (0.24 ± 0.07), V_{MP} (0.24 ± 0.09) and W_d (1.86 ± 0.37). A temperature change from 60 to 100 °C resulted in increases for all these properties. No significant temperature effect was observed for V_{mp}. Since the factorial design results are incomplete for the AS, Calc and *b* measurements, their effect values could not be calculated. No other significant effect values were calculated for any of these properties except for a significant 90% confidence level ethanol effect on S_{BET}. On average the presence of ethanol seems to increase the value of S_{BET}.

Positive 95% confidence level effects of changing both the HCl concentration and temperature were found for the thermogravimetric results. On the average increased quantities of SiO_2–H_2O, SiO_2, SiOH and ≡SiOH mmol OH g^{-1} SiO_2 were found on raising the temperature from 60 to 100 °C. Increasing the HCl concentration from 0.2 to 2.0 mol L^{-1} increased the quantities of SiO_2–H_2O, SiO_2 and SiOH, but ≡SiOH mmol OH g^{-1} SiO_2 did not show a significant main concentration effect. However, a 95% level significant positive interaction effect between temperature and HCl concentration was found for this response.

A graph of the first two principal component loadings for the factorial design is presented in Fig. 4.

All the textural, structural and thermogravimetric responses as well as the experimental factors were included in the calculation. This two dimensional plot contains 71.4% of the total data variance. Note that S_{BET}, V_{MP}, V_{PT}, Calc and W_d besides all the thermogravimetric responses have negative response values for the first principal component, as does the temperature. This indicates that these properties are all correlated with temperature. The *b* value has the most positive first principal component loadings and is negatively correlated the temperature. The 60–100 °C temperature change tends to reduce the *b* values for these experiments whereas it increases the other textural, structural and thermogravimetric responses except for V_{mp} and AS since they have first principal component loadings close to zero and, as such, are not expected to be affected by temperature. The decrease of *b* with the increase of temperature is related to the density increase of the pore walls.

Fig. 5 shows the score plot for the first two principal components. Each experiment is indicated in the graph by the sign convention used in Tables 1 and 3.

Note that all the experiments with 100 °C temperature are on the left of the score graph (indicated by a positive sign for the last sign in the sign combination) and the S_{BET}, V_{MP}, V_{PT}, Calc and W_d properties and the thermogravimetric results are on the left side of the loading graph. This is consistent with positive temperature effects for all these responses since these variables are all positively correlated. Experiments at 60 °C are represented by points on the right side of the score graph, corresponding to the *b* response point on that side of the loading graph. On average the *b* values are higher for these experiments at the lower temperature. The HCl concentration has a negative loading for the second principal component and is negatively correlated with the S_{BET}, V_{PT} and V_{MP} responses that have positive loadings. As such one can expect experiments carried out with a 0.2 M HCl concentration to have higher results than those employing the higher HCl concentration. This can be confirmed in Table 2 for experiments with the same temperature value and ethanol factor levels. There are exceptions but usually an HCl concentration increase corresponds to a decrease in the S_{BET}, V_{PT} and V_{MP} values, other factors being maintained at the same level. On the other hand SiO_2–H_2O and SiO_2 have loading points close to the HCl concentration point. Hence all their values are expected to be positively correlated indicating positive HCl concentration effects on SiO_2–H_2O and SiO_2. Indeed results for the experiments in Table 4 corresponding to the higher HCl concentration always have higher SiO_2–H_2O and SiO_2 contents if their temperature and ethanol levels are the same. As a result experiments with the lower HCl concentration, as indicated by an initial negative sign in the sign combinations representing the experiments in the score graph in Fig. 5, have positive second principal component scores whereas experiments carried out at 2.0 M HCl have score points in the lower portion of the graph. In order to fully evaluate the effect of HCl concentration, the formation of ordered mesopores has to be considered. For instance, samples number 7 and 7*b*, prepared with a lower HCl concentration did not present ordered mesopores.

Table 3
Adsorption, structural and textural parameters for the calcined FDU-1 samples. Data from the N_2 adsorption isotherm at −196 °C and SAXS data for the full 2^3 factorial design.

Experiments	Textural proprieties				Structural properties			
	S_{BET} ($m^2\ g^{-1}$)	V_{PT} ($cm^3\ g^{-1}$)	V_{MP} ($cm^3\ g^{-1}$)	V_{mp} ($m^2\ g^{-1}$)	AS a (nm)	Calc a (nm)	W_d (nm)	b (nm)
1 (− − −)	436	0.46	0.37	0.086	21.4	18.5	7.6	5.2
2 (+ − −)	361	0.40	0.32	0.084	20.4	18.1	7.7	5.7
3 (− + −)	432	0.44	0.35	0.089	19.9	17.4	7.5	5.1
4 (+ + −)	399	0.40	0.31	0.092	20.9	17.2	7.6	5.6
5 (− − +)	536	0.64	0.54	0.101	21.9	17.4	9.4	3.7
6 (+ − +)	476	0.55	0.44	0.108	22.3	19.6	9.4	3.9
7 (− + +)	491	0.50	0.39	0.107	–	–	7.2	–
8 (+ + +)	577	0.73	0.62	0.091	20.8	20.3	9.7	3.7
1B (− − −)	424	0.47	0.37	0.098	23	19.7	7.1	5.6
2B (+ − −)	337	0.35	0.27	0.085	21.4	17.4	7.6	6.3
3B (− + −)	557	0.69	0.63	0.063	20.9	17.3	7.2	3.0
4B (+ + −)	392	0.41	0.32	0.086	19.9	16.9	7.3	5.4
5B (− − +)	524	0.61	0.57	0.038	21.7	20.4	9.4	3.7
6B (+ − +)	528	0.67	0.56	0.114	22.6	20.1	9.9	3.3
7B (− + +)	757	1.00	0.99	0.012	–	–	10.0	–
8B (+ + +)	617	0.80	0.71	0.112	21.5	20.1	9.5	2.9

S_{BET}, specific surface área; V_{TP}, total pore volume; V_{MP}, mesopore volume; V_{mp}, micropore volume; a, lattice parameter, AS, as-synthesized; Calc, calcined; W_d, pore width; b, wall thickness.

Table 4
Thermogravimetric data obtained for the next-to-last and final mass losses of factorial design samples expressed as amounts of silanol groups (mmol g^{-1} SiO_2).

Experiments	$SiO_2{\cdot}nH_2O$ (%)	SiO_2 (%)	≡Si–OH (%)	≡Si–OH (mmol g^{-1} SiO_2)
1 (− − −)	37.6	36.7	1.7	2.7
2 (+ − −)	54.3	53.4	1.7	1.9
3 (− + −)	36.4	35.7	1.3	2.2
4 (+ + −)	53.8	52.5	2.5	2.4
5 (− − +)	52.3	50.8	2.8	3.3
6 (+ − +)	56.1	54.9	2.3	2.4
7 (− + +)	52.7	51.7	1.9	2.2
8 (+ + +)	56.1	53.9	4.2	4.5
1B (− − −)	44.0	42.8	2.3	3.2
2B (+ − −)	62.4	61.1	2.9	2.7
3B (− + −)	40.6	39.4	2.3	3.4
4B (+ + −)	49.6	48.7	1.9	2.3
5B (− − +)	56.0	54.5	2.9	3.1
6B (+ − +)	65.8	63.8	3.8	3.5
7B (− + +)	50.4	48.9	2.9	3.5
8B (+ + +)	68.5	65.3	6.0	5.4

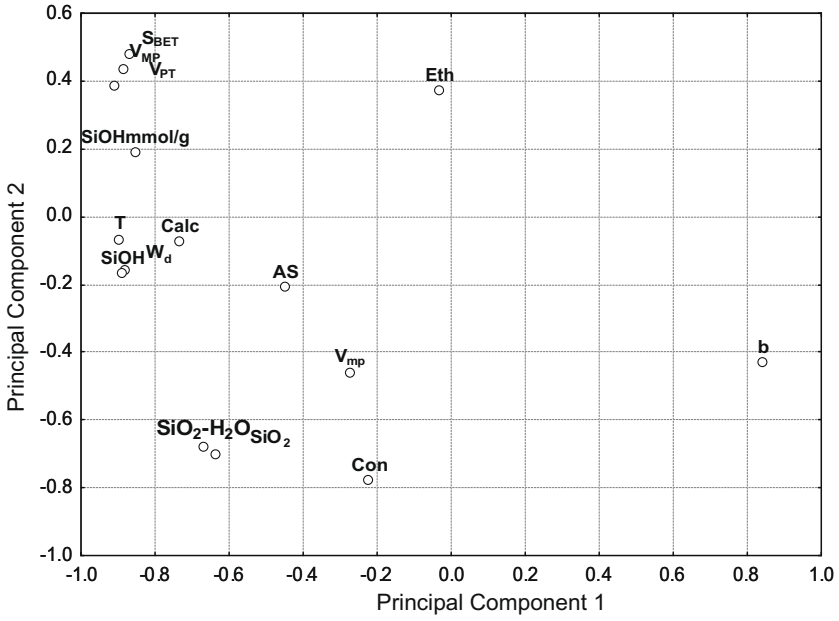

Fig. 4. Loading graph for the first two principal components for the 2^3 factorial design results. Textural, structural and thermogravimetric response values and experimental factor levels have been included in the calculation.

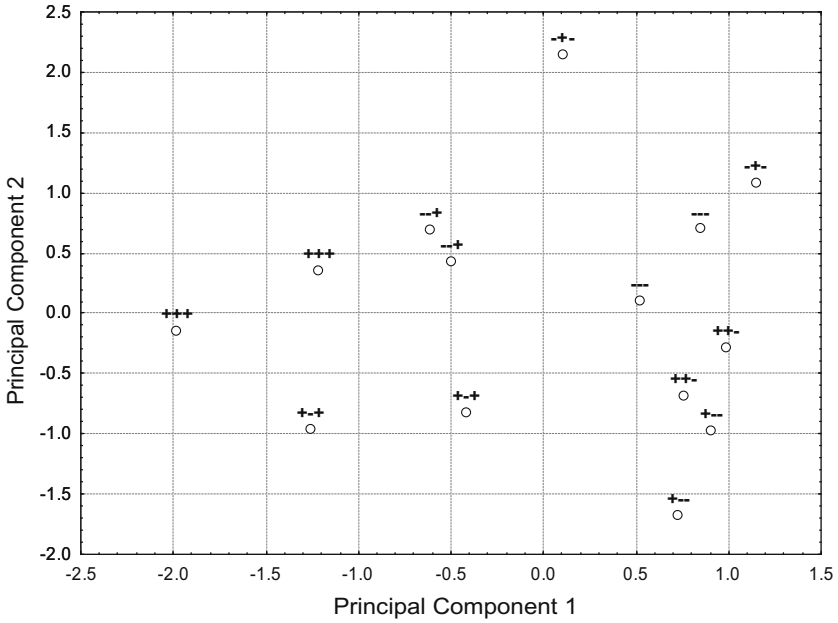

Fig. 5. Score graph for the first two principal components for the 2^3 factorial design results. Textural, structural and thermogravimetric response values and experimental factor levels have been included in the calculation.

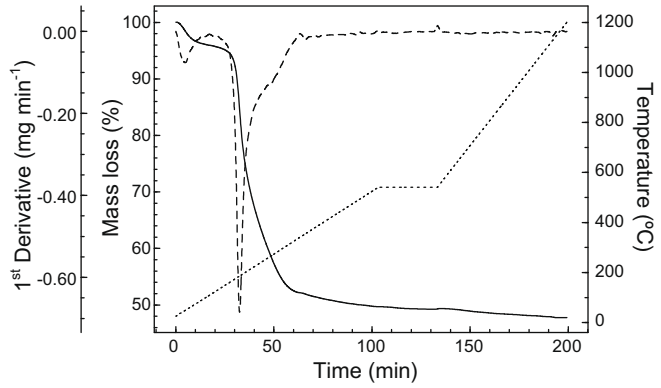

Fig. 6. TG/DTG/T results obtained for sample number 4 of the central composite design.

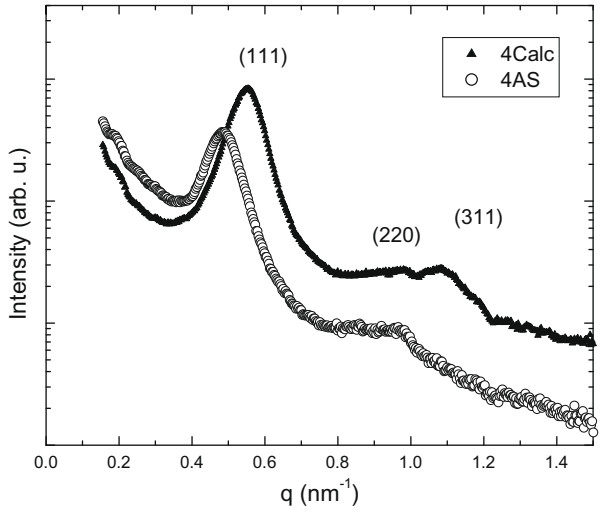

Fig. 7. Small angle X-ray scattering (SAXS) patterns for as-synthesized and calcined sample number 4 of a central composite design.

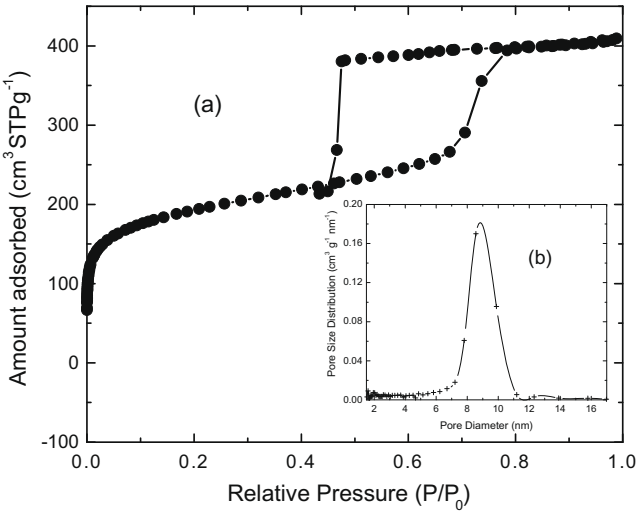

Fig. 8. (a) Nitrogen sorption isotherm at −196 °C and (b) the corresponding pore size distributions for sample number 4 of the central composite design.

To analyze the effects of stirring time and microwave exposure time on the microwave-assisted synthesis of FDU-1 silica a central composite design was carried out. Fig. 6–8 are typical TG/DTG/T, SAXS and N_2 sorption data of this set of samples. The stirring and microwave exposure times are presented in Table 2 along with their codified values, designated as X_1 and X_2. Table 5 contains the textural and structural properties determined for each central composite design experiment whereas Table 6 presents the thermogravimetric results.

Linear and quadratic models for each response as a function of stirring and microwave exposure times were calculated in order to evaluate their linear and quadratic effects on the responses. A significant linear effect of stirring time on S_{BET} and significant linear and quadratic effects of microwave exposure time were found for AS. The principal component loading graph is shown in Fig. 9. In the upper right corner the AS, V_{mp} and b responses are clustered

Table 5
Adsorption, structural and textural parameters for the calcined FDU-1 samples. Data from the N_2 adsorption isotherm at −196 °C and SAXS data for the central composite design.

Experiments	Textural properties				Structural properties			
	S_{BET} ($m^2\ g^{-1}$)	V_{TP} ($cm^3\ g^{-1}$)	V_{MP} ($cm^3 g^{-1}$)	V_{mp} ($m^2\ g^{-1}$)	AS a (nm)	Calc a (nm)	W_d (nm)	b (nm)
1 (− −)	515	0.56	0.47	0.09	21.5	16.8	7.5	3.9
2 (+ −)	622	0.68	0.59	0.09	21.5	17.9	8.5	3.5
3 (− +)	516	0.53	0.42	0.11	21.9	17.9	8.7	4.7
4 (+ +)	646	0.63	0.50	0.13	22.5	19.6	8.6	4.6
5 (0 0)	647	0.73	0.63	0.10	21.8	19.1	10.1	3.6
6 (0 0)	594	0.57	0.44	0.13	21.7	17.4	8.5	4.6
7 (0 0)	550	0.57	0.46	0.11	21.5	18.0	8.6	4.2
8 ($-\sqrt{2}$ 0)	520	0.54	0.44	0.10	21.6	17.4	8.7	4.4
9 (0 $\sqrt{2}$)	605	0.58	0.44	0.14	22.5	18.2	8.6	4.8
10 ($\sqrt{2}$ 0)	714	0.70	0.55	0.15	21.6	18.5	8.5	4.1
11 (0 $-\sqrt{2}$)	655	0.62	0.51	0.11	22.0	18.3	10.6	4.1

S_{BET}, specific surface área; V_{TP}, total pore volume; V_{MP}, mesopore volume; V_{mp}, micropore volume; a, lattice parameter, AS, as-synthesized; Calc, calcined; W_d, pore width; b, wall thickness.

Table 6
Thermogravimetric data obtained from the mass losses of central design samples expressed as amounts of silanol groups (mmol ≡ SiOH g^{-1}.SiO_2).

Experiments	$SiO_2.nH_2O$ (%)	SiO_2 (%)	H_2O (%)	≡Si–OH (mmol g^{-1} SiO_2)
1 (− −)	48.7	47.7	1.0	2.3
2 (+ −)	51.7	50.6	1.1	2.5
3 (− +)	51.1	50.1	1.0	2.1
4 (+ +)	51.4	49.8	1.6	3.8
5 (0 0)	50.6	48.8	1.8	4.3
6 (0 0)	51.0	49.7	1.3	3.1
7 (0 0)	48.2	47.2	1.0	2.0
8 ($-\sqrt{2}$ 0)	48.8	47.4	1.4	3.1
9 (0 $\sqrt{2}$)	49.4	48.0	1.4	3.1
10 ($\sqrt{2}$ 0)	49.5	47.6	1.9	4.4
11 (0 $-\sqrt{2}$)	56.6	55.5	1.1	2.9

close to microwave exposure time indicating that this factor tends to have positive effects on these response values. This was indeed found to be the case for AS by response surface methodology. A quadratic function fits the AS response values in terms of stirring time and microwave exposure time. This model shows no lack of fit at the 95% confidence level and significant positive linear and quadratic effects of microwave exposure time on AS. Another group of points is clustered close to the stirring time and can be expected to be correlated with it. This was found to be true for S_{BET} by the response surface methodology. Linear and quadratic models were both found to fit the S_{BET} response values with no lack of fit. The only significant regression coefficient (at the 90% confidence level) was the positive linear effect of stirring time on S_{BET}. As such one can expect experiments with longer stirring times to correspond to higher values of S_{BET}, V_{MP}, V_{PT}, Calc, ≡SiOH (mmol g^{-1}) and H_2O.

The corresponding score graph is shown in Fig. 10 where points are identified by the codified experimental conditions in Table 2. The first principal component tends to be associated with stirring time, all the shortest stirring time experiments are on the extreme right and the longer times are toward the left. Experiments carried out with more than 20 min. stirring time all resulted in larger S_{BET}, V_{PT}, V_{MP} and Calc values. The tendency appears to hold for H_2O and SiOH but experimental error can be expected to perturb the trends.

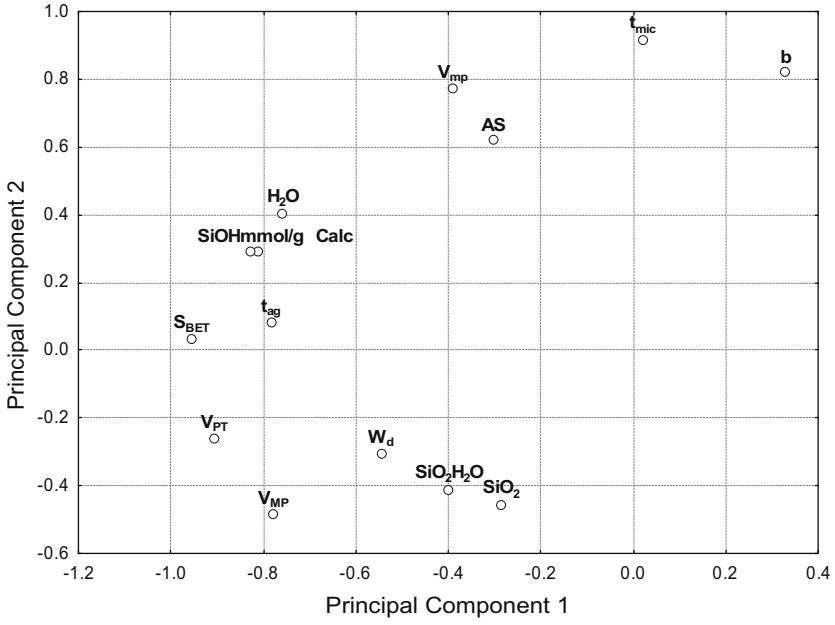

Fig. 9. Loading graph for the first two principal components for the central composite design. Textural, structural and thermogravimetric response values and experimental factor levels have been included in the calculation.

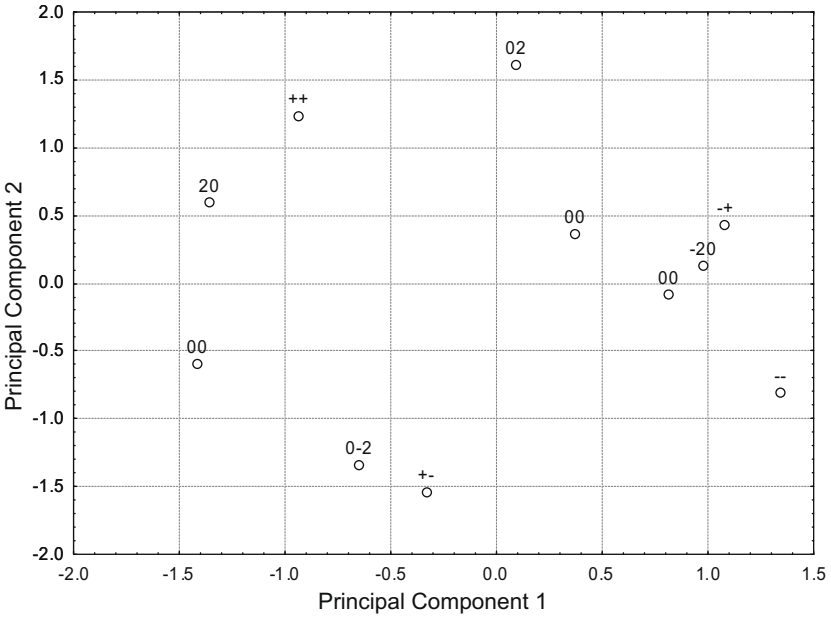

Fig. 10. Score graph for the first two principal components for the central composite design results. Textural, structural and thermogravimetric response values and experimental factor levels have been included in the calculation.

Results with high microwave exposure times tend to occupy the upper portion of the graph whereas experiments with short exposure times are represented by points near the bottom. Hence the second principal component is correlated with microwave exposure time. Longer exposure times tend to produce higher AS, V_{mp} and b response values. The experiments carried out with the longest exposure time, 132 min, resulted in the largest b and AS values and the second largest V_{mp} value. Large values are also found for experiments with a 120 min exposure time.

4. Summary

The three analyzed factors of the full 2^3 factorial design: hydrothermal temperature, dissolution in ethanol and HCl concentration showed that higher temperature, copolymer dissolution in ethanol and higher HCl concentration induces better structural/textural properties of the mesoporous ordered silica. The 2^2 central composite design showed better structural properties for longer stirring time, therefore, promoting an increase of siliceous species around the template. On the other hand, longer microwave-assisted hydrothermal treatment times increased the pore wall thickness, but induced larger amounts of micropores, which is a deleterious effect. As such an optimized synthesis of FDU-1 silica with Vorasurf 504® can be performed based on the optimized conditions found in this study. In fact, samples numbered 8 and 8*B* were synthesized at these optimum conditions (2.0 mol L^{-1} HCl, ethanol dissolution, hydrothermal microwave-assisted synthesis temperature of 100 °C, stirring time of 24 h and 60 min of hydrothermal microwave-assisted synthesis time).

Acknowledgments

Thanks are due to FAPESP (L.C. Cides da Silva, Grants 03/10067-3, 2007/07646-2), CNPq and CAPES, for financial support. LNLS (Brazilian Synchrotron Light Laboratory, Brazil, proposals D11A-SAXS 2795 and 5315) is also acknowledged. The authors thank Prof. Elizabeth de Oliveira and Prof. Pedro Vitoriano de Oliveira from LEEAA/IQ-USP for the use of their microwave oven.

References

[1] G.T. Kokotailo, S.L. Lawton, D.H. Olson, W.M. Méier, Nature 272 (1978) 437.
[2] C.T. Kresge, M.E. Leonowics, W.J. Roth, J.C. Vartulli, J.S. Beck, Nature 359 (1992) 710.
[3] J.S. Beck, J.C. Vartulli, W.J. Roth, M.E. Leonowics, C.T. Kresge, K.D. Schmidt, W. Chu, D.H. Olson, E.W. Sheppard, S.B. McCullen, J.B. Higgins, J.L. Schlenker, J. Am. Chem. Soc. 114 (1992) 10834.
[4] D.Y. Zhao, J.L. Feng, Q.S. Huo, N. Melosh, G.H. Fredrickson, B.F. Chmelka, G.D. Stucky, Science 279 (1998) 548.
[5] D.Y. Zhao, Q.S. Huo, J.L. Feng, B.F. Chmelka, G.D. Stucky, J. Am. Chem. Soc. 120 (1998) 6024.
[6] C. Yu, Y. Yu, D. Zhao, Chem. Commun. (2000) 575.
[7] C. Yu, B. Tian, J. Fan, G.D. Stucky, D. Zhao, J. Am. Chem. Soc. 124 (2002) 4556.
[8] M. Kruk, E.B. Celer, M. Jaroniec, Chem. Mater. 16 (2004) 698.
[9] D.G. Choi, S.M. Yang, J. Colloid Interf. Sci. 261 (2003) 127.
[10] T. Yu, H. Zhang, X. Yan, Z. Chen, X. Zou, P. Oleynikov, D. Zhao, J. Phys. Chem. B 110 (2006) 21467.
[11] Z.W. Jin, X.D. Wang, X.G. Cui, J. Colloid Interface Sci. 307 (2007) 158.
[12] M.C.A. Fantini, J.R. Matos, L.C. Cides da Silva, L.P. Mercuri, G.O. Chiereci, E. Celer, M. Jaroniec, Mat. Sci. Eng. B. 112 (2004) 106.
[13] L.C. Cides da Silva, T.S. Martins, M.S. Filho, E.E.S. Teotonio, P.C. Isolani, H.F. Brito, M.H. Tabacniks, M.C.A. Fantini, J.R. Matos, Micropor. Mesopor. Mater. 92 (2006) 94.
[14] R.M. Grudzien, B.E. Grabicka, M. Kozak, S. Pikus, M. Jaroniec, New J. Chem. 30 (2006) 1071.
[15] L.C. Cides da Silva, L.B.O. dos Santos, G. Abate, I.C. Cosentino, M.C.A. Fantini, J.C. Masini, J.R. Matos, Micropor. Mesopor. Mater. 110 (2008) 250.
[16] J. Estella, J.C. Echeverrıa, M. Laguna, J.J. Garrido, J. Non-Cryst. Solids 353 (2007) 286.
[17] G. Øye, J. Sjöblom, M. Stöcker, Micropor. Mesopor. Mater. 34 (2000) 291.
[18] T. Klimova, A. Esquivel, J. Reyes, M. Rubio, X. Bokhimi, J. Aracil Stöcker, Micropor. Mesopor. Mater. 93 (2006) 331.
[19] M. Moliner, J.M. Serra, A. Corma, E. Argente, S. Valero, V. Botti, Micropor. Mesopor. Mater. 78 (2005) 73.
[20] E. Dumitriu, D. Lutic, V. Hulea, D. Dorohoi, A. Azzouz, E. Colnay, C. Kappenstein, Micropor. Mesopor. Mater. 31 (1999) 187.
[21] J.A. Cornell, in: S.S. Shapiro, E.F. Mykytka (Eds.), The ASQC Basic References in Quality Control: Statistical Techniques, American Society for Quality Control, Milwalkee, WI, EUA, 1990.
[22] R.H. Myers, D.C. Montgomery, Response Surface Methodology: Process and Product Optimization Using Designed Experiments, Willey, New York, 1995.
[23] G.E.P. Box, J.S. Hunter, W.G. Hunter, Statistics for Experimenters, Wiley Interscience, Hoboken, NJ, 2005.
[24] R.E. Bruns, I.S. Scarminio, B. de Barros Neto, Statistical Design – Chemometrics, Elsevier, Amsterdam, 2006.
[25] R. Reeyment, K.G. Joreskog, Applied Factor Analysis in the Natural Sciences, Cambridge University Press, Cambridge, 1993.
[26] M.A. Sharaf, D.L. Illman, B.R. Kowalski, Chemometrics, Wiley, NY, 1986.
[27] G. Kellermann, F. Vicentin, E. Tamura, M. Rocha, H. Tolentino, A. Barbosa, A. Craievich, I. Torriani, J. Appl. Crystallogr. 30 (1997) 880.

[28] A.F. Craievich, Mater. Res. 5 (2002) 1–11.
[29] S. Brunauer, P.H. Emmet, E. Teller, J. Am. Chem. Soc. 60 (1938) 309.
[30] E.P. Barret, L.G. Joyner, P.H. Halenda, J. Am. Chem. Soc. 73 (1951) 309.
[31] M. Kruk, M. Jaroniec, A. Sayari, Langmuir 13 (1997) 6267.
[32] P.I. Ravikovitch, A.V. Neimark, Langmuir 18 (2002) 1550.
[33] J.R. Matos, M. Kruk, L.P. Mercuri, M. Jaroniec, L. Zhao, T. Kamiyama, O. Terazaki, T.J. Pinnavaia, Y. Liu, J. Am. Chem. Soc. 125 (2003) 821.
[34] K. Kruk, Ewa B. Celer, M. Jaroniec, Chem. Mater. 16 (2004) 698.